applied optics

Enabling focusing around the corner in multiple scattering media

Saara-Maarit Reijn,[1,2,*] Felipe A. Pinheiro,[3,4] Dimitri Geskus,[1,2] and Niklaus U. Wetter[1]

[1]Centro de Lasers e Aplicações, Instituto de Pesquisas Energéticas e Nucleares, Av. Prof. Lineu Prestes 2242, 05508-000 São Paulo, Brazil
[2]Department of Materials and Nano Physics, KTH Royal Institute of Technology, Isafjordsgatan 22, 16440 Kista, Sweden
[3]Instituto de Física, Universidade Federal do Rio de Janeiro, 21941-972 Rio de Janeiro, Brazil
[4]Optoelectronics Research Center and Center for Photonic Metamaterials, University of Southampton, Highfield, Southampton SO17 1BJ, UK
*Corresponding author: reijn@kth.se

Received 16 June 2015; revised 10 August 2015; accepted 10 August 2015; posted 11 August 2015 (Doc. ID 243107); published 28 August 2015

We report an alternative experimental setup to laterally focus light at an angle of 90 deg relative to turbid, multiple scattering media, using preprocessing wavefront shaping. We compare the measured image quality to one obtained in the usual configuration for focusing light through turbid media, where focusing occurs behind the scattering sample. We demonstrate that the depth of focus in the lateral configuration is of the same order of the usual transversal one because both setups are designed to operate in the deep Fresnel zone. This result shows that this novel, versatile lateral configuration allows for effectively focusing around corners through multiple scattering samples.

OCIS codes: (030.6140) Speckle; (110.6150) Speckle imaging; (120.6150) Speckle imaging; (120.7000) Transmission; (290.1990) Diffusion; (290.4210) Multiple scattering.

http://dx.doi.org/10.1364/AO.54.007740

1. INTRODUCTION

Multiple light scattering is a ubiquitous phenomenon, as it occurs in many different natural complex media, such as clouds, planetary atmosphere, biological tissues, and colloids [1]. It also encloses rich physical phenomena, as many mesoscopic effects in condensed matter have optical counterparts in strong light scattering systems, such as the weak and strong (Anderson) localization of light and anomalous diffusion [1,2].

In addition to the fundamental interest, disorder in optical systems, which in principle could be considered as a nuisance, is exploited in many applications. Well-known examples are random lasers, where disorder provides the optical feedback and plays the role of mirrors in conventional lasers [3]. Another important example is imaging through turbid media, which is crucial for deep tissue imaging [4]. However, the fact that multiple scattered light generates complex time-dependent speckle patterns makes use of adaptive-optics techniques to correct aberrations unpractical [5]. The demonstration that the effects of disorder and multiple scattering can be partially compensated by controlling the phase front of the incident light, restoring the focal spot, has created a new paradigm in imaging through turbid media [6–8]. Wavefront shaping is achieved by using a spatial light modulator (SLM) so that the incident beam matches the transmission eigenmodes of the scattering sample. This technique has been employed in many applications, including astronomical and biological imaging [7], fluorescence microscopy [9], subdiffraction limit focusing [7], focusing and compression of ultrashort pulses [10], spectral filtering [11], light polarization control [12], random lasing [13], and focusing behind fully reflective materials [14].

In all these applications of the wavefront shaping method, the scattering media and feedback system need to be properly aligned with the target sample. In the present paper, we propose a novel, alternative experimental setup to focus light through turbid media using wavefront shaping. Within this configuration, focusing occurs laterally to the scattering sample and not behind it, as in the usual setup. This should facilitate applications involving imaging [15] and micromanipulation [16] with samples on nontransparent substrates.

Imaging around corners has been reported in the past and is often associated to imaging occluded objects by reflection at an angle from diffuse surface using the time-of-flight method [17] or correcting the reflected wavefront (postprocessing) by means of a SLM [18]. Imaging around corners in transmission mode has been suggested [19] using postprocessing with SLM but never actually demonstrated. Here we show, for the first time to our knowledge, focusing around a corner at a 90 deg angle by transmission through a diffuse object, using preprocessing of the impinging wavefront with a SLM.

We compare the quality of focusing in the lateral and the usual (transversal) configuration of the same order of the usual,

transversal one; we show that this novel, versatile configuration allows for effectively focusing around corners.

2. METHODOLOGY

A. Transversal Focusing Configuration

Before describing the experimental setup used to focus light around the corner, let us begin by briefly explaining the setup that has been used so far to focus light through turbid media, the transversal focusing configuration [19], which is shown in Fig. 1. The phase of the impinging beam is modulated by a spatial light modulator (SLM). The modulated light is focused onto a Teflon sample, S, of 2 mm thickness, having a transport mean free path of 600 μm (measured via the width of the coherent backscattering cone). The light traveling through and scattered by the Teflon sample is collected by an imaging system consisting of an objective lens and a CCD camera. The speckle pattern is captured, and a region of interest (ROI) in the center of the CCD camera is selected. The intensity of the light collected by the ROI is enhanced by means of a feedback algorithm that controls the SLM with help of a computer program in LabVIEW. The stepwise sequential algorithm, as described by Vellekoop and Mosk [19], is used to look for a phase mask that focuses light through the Teflon sample. This algorithm is based on the fact that the field at the detector is a linear superposition of the contributions from all squared segments that constitute the modulator. Hence, the optimal wavefront is constructed by optimizing each of the segments individually, as a computer varies the phase of each segment from 0 to 2π. Then, the feedback signal is monitored and the phase for which the target intensity is maximal is recorded. The optimal wavefront is constructed such that the contribution of this single segment is in phase with the background field (the mean contribution coming from all other segments).

B. Lateral Focusing Configuration

The experimental setup for focusing in the lateral configuration is the same as for focusing in the transversal configuration, with the difference being that the objective lens and CCD camera are now positioned to look at the Teflon sample under a 90 deg angle from the side, rather than the back, as is shown by Fig. 2. The Teflon sample has been replaced with a thicker one, allowing for better alignment of the imaging system with the illuminated region.

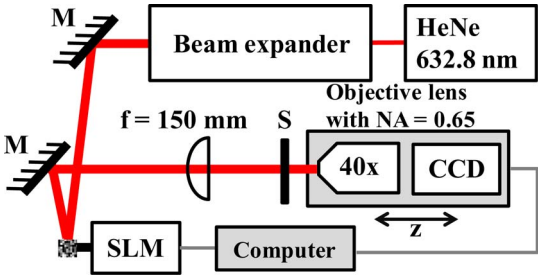

Fig. 1. Schematic of the experimental setup for focusing in the transversal configuration.

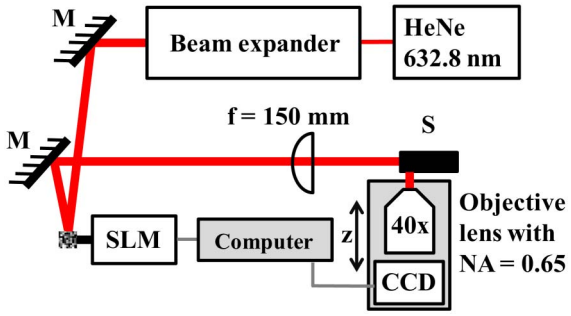

Fig. 2. Schematic of the experimental setup for focusing in the lateral configuration.

3. EXPERIMENTAL DETAILS

The experimental setup, as shown in Fig. 1, was built. After measurements were performed, the experimental configuration was set to the lateral configuration, as shown in Fig. 2. A low power (~4 mW), linearly polarized, and stabilized He–Ne laser with 632.8 nm wavelength was expanded by a plano–concave and plano–convex lens (focal lengths of −30 and 250 mm, respectively) to expand the laser beam to illuminate the full modulated (Holoeye Pluto phase only, 1920 × 1080 pixels) SLM head. Because the SLM head only accepts horizontal polarized light, the He–Ne laser tube was turned to correspond to the same polarization. The iteration time (i.e., time needed to cycle through 10 phase steps for one SLM segment) is 3.33 s. The phase modulated light is focused onto the Teflon sample by a plano–convex lens with a 150 mm focal length. The light scattered by the Teflon sample is collected by an imaging system consisting of a 40× magnifying objective lens with a numerical aperture (NA) of 0.65, finite corrected at 170 mm, and a (Thorlabs DCU223M, 1024 × 768 pixels) CCD camera fixed at a position of 170 mm behind the objective lens, to collect the light. Alignment of the imaging system is realized by first imaging the Teflon sample surface on the CCD camera and then translating the imaging system back by a distance of a few mm, which we call the focal length of the scattering lens and denote by z_0 [7]. This imaging system has a lateral resolution of 0.48 μm (FWHM), limited by the NA of the objective lens. The speckle pattern is captured by the CCD, and a 5 × 5 pixels square ROI in the center of the CCD camera is selected in order to focus and enhance light by means of a feedback algorithm. The ROI is chosen to be just above the system resolution limit, which is 5 pixels (pixel size 4.65 μm × 4.65 μm).

A. Feedback Algorithm Settings

The feedback algorithm parameters used to address the SLM and read out the CCD are listed in Table 1. The pixels on the SLM were binned together to form large $s \times s$ pixels square segments. This results in a lesser total number of segments, N, to cycle through, which significantly speeds up the algorithm and thereby reduces the measurement time. It takes about 11 min to obtain focus when using 196 segments.

Table 1. Measurement Parameters for Feedback Algorithm

Parameter	Value	Unit
s	35	Pixels
N	196	Segments
phase steps	10	–
ROI_{CCD}	5	Pixels

Table 2. Enhancement Results for Four Consecutive Lateral Focusing Measurements

Measurement	Enhancement Factor [-]	I_{ROI} [Gray Level]
a	10	11
b	13	7
c	18	5
d	21	6

4. RESULTS

A. Focusing Around the Corner

Four consecutive measurements have been performed to test the rigidity of the focusing capabilities when focusing in the lateral configuration (i.e., around the corner). The results are shown in Fig. 3. The focal spot images are cropped to improve the visibility of the spots.

Table 2 lists the enhancement factors (i.e., the ratio between the optimized intensity and the average intensity before optimization [6]) obtained for the focal spots. The lower enhancement factors found here compared with the enhancement factors of the order of 1000 obtained in [6] can probably be explained by the lower stability of our setup. Table 2 also lists the initial average intensity of the CCD's ROI, I_{ROI}, prior to starting the optimization procedure. The difference in enhancement factors is caused by the initial average intensity in the ROI of the CCD. With an I_{ROI} of around 10, the enhancement factors are limited to about 10. For enhancement factors around 20, the I_{ROI} started off with twice a lower value. The starting value of the ROI for the optimization procedure has a lower limit governed by the noise floor level and determines how high the enhancement factor can be expected.

The enhancement factor for measurement c is expected to be higher, when referring to the aforementioned trend. However, when we look at the phase masks, shown in Fig. 4 (especially for a–c), we see that a significant part on the left side is black, meaning that the optimization procedure failed to find a phase for these segments. The optimization procedure does fail due to diverse reasons. For example, it fails because the system persistence time is not always long enough, as shown in the case of transverse focusing [see transversal phase-mask of Fig. 6(b)]. In addition, light impinging the SLM on the left side travels a longer distance through the Teflon sample; therefore, it is not being collected by the imaging system. This makes the phase mask effectively smaller (i.e., utilizing fewer segments

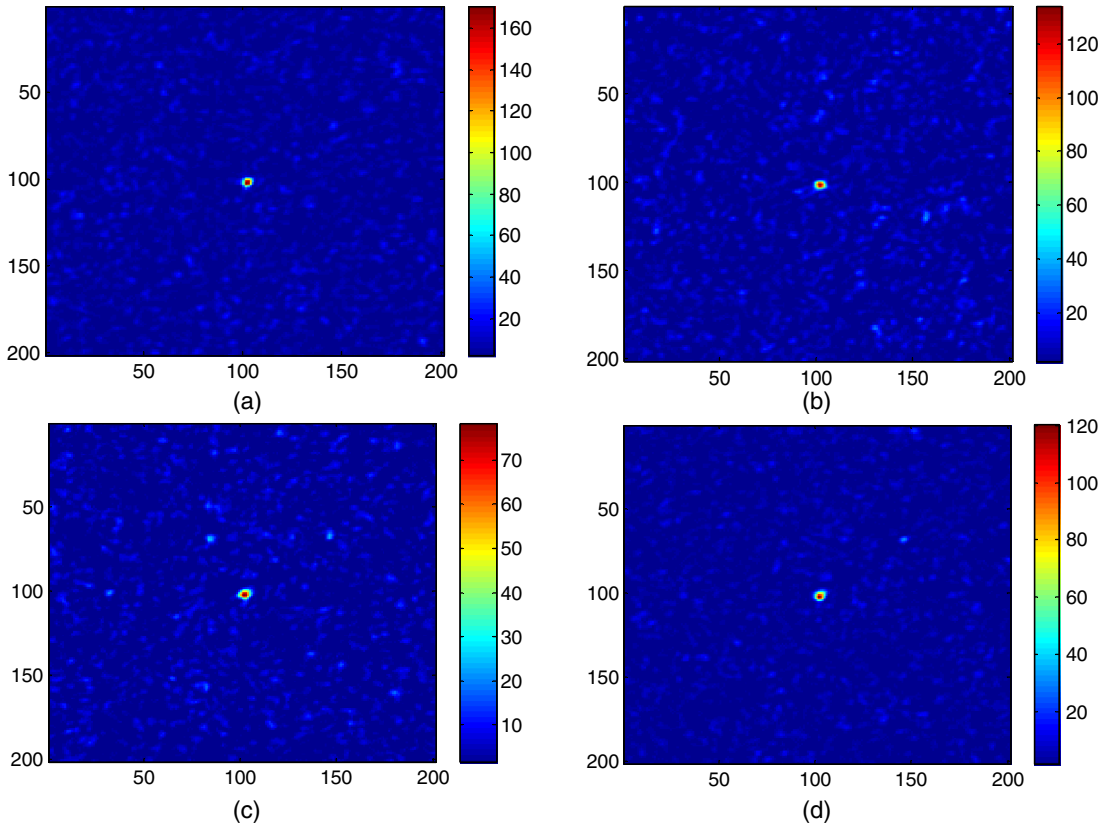

Fig. 3. (a)–(d) Cropped images of focal spots obtained for lateral focusing (i.e., around the corner). Enhancement factors are (a) 10, (b) 13, (c) 18, and (d) 21. The axes denote the pixels of the CCD.

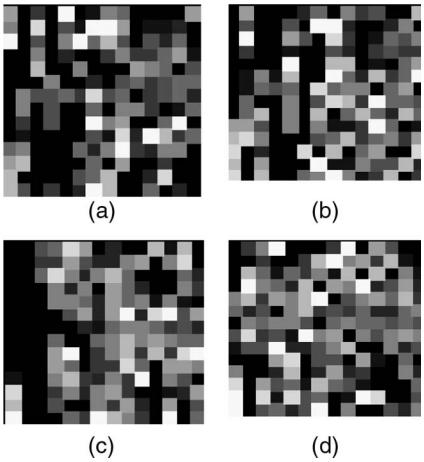

Fig. 4. (a)–(d) Phase masks obtained for lateral focusing.

in the optimization procedure and hence reducing the enhancement factor [6]).

B. Comparison of Focusing Quality for Transversally and Laterally Obtained Foci

We qualitatively compare the transversal and lateral focusing quality by comparing the focal widths and depth of foci. The feedback algorithm parameters used to address the SLM and read out the CCD are the same as listed in Table 3.

The diameter of the illuminated area on the back end of the Teflon scattering lens, D_2, is determined for the transversal and lateral focusing configuration from Fig. 5.

Figure 6 shows the resulting phase masks used to focus light laterally and transversally through the Teflon scattering lens. The correspondingly obtained focal spots are shown in Fig. 7. The laterally and transversally obtained foci have an enhancement factor of 18 and 7 with $I_{\mathrm{ROI,lateral}} = 2$ and $I_{\mathrm{ROI,transversal}} = 9$, respectively.

The focal length of the scattering Teflon lens, z_0, is noted for both focusing configurations and is listed in Table 4. Therefore, the plane shown in Fig. 7, which contains the speckle and the focus imaged onto the CCD, is formed at a distance z_0 from the Teflon sample. In order to start the feedback algorithm, enough light has to be collected to overcome the noise floor level of the setup [6,20]. Therefore, the z_0 in the lateral configuration is chosen smaller than the z_0 in the transversal experiment to collect sufficient light onto the CCD.

The width of the focal spot, w_0, is experimentally determined by taking the full width at half maximum (FWHM) of the focal spot. The line scans through the focal spots are depicted in Fig. 8. The focal width is determined by taking

Table 3. Measurement Parameters for Feedback Algorithm

Parameter	Value	Unit
s	10	Pixels
N	100	Segments
Phase steps	10	–
$\mathrm{ROI_{CCD}}$	5	Pixels

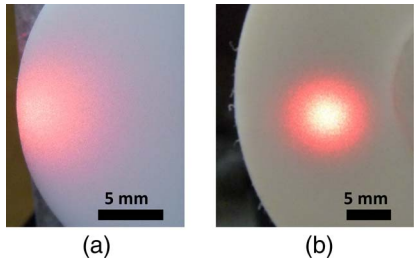

Fig. 5. Illuminated area, D_2, (a) in lateral direction, laser beam impinging from the left, and (b) transversal direction, laser beam impinging from behind.

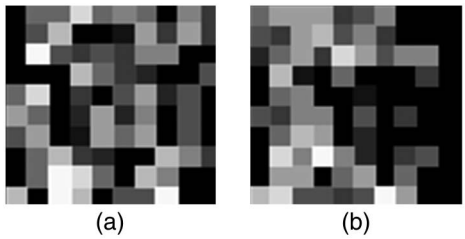

Fig. 6. Phase masks obtained for (a) lateral focusing and (b) transversal focusing.

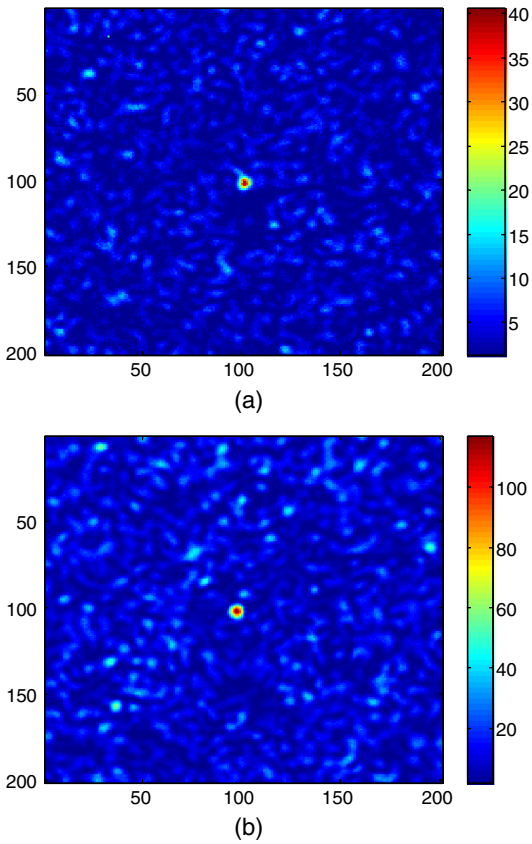

Fig. 7. Cropped images of focal spots obtained for (a) lateral focusing and (b) transversal focusing. Enhancement factors are (a) 18 and (b) 7. The axes denote the pixels of the CCD.

Table 4. Experimental Details for Transversal and Lateral Focusing Configuration

	Configuration	
Parameter	Transversal (mm)	Lateral (mm)
D_2	~7.0	~7.5
z_0	2	0.5

the FWHM of these two scans (through the x and y axes) and averaging the results. The focal width is found to be (0.6 ± 0.1) μm and (0.7 ± 0.1) μm for the lateral and transversal configuration, respectively. The error margin is governed by the read-off error, which can be no more than the distance between two pixels.

The depth of focus for Gaussian beams is a measure to express how fast the beam diverges around the focal plane. This is expressed by the Rayleigh length, z_R:

$$z_R = \frac{\pi w_0^2}{\lambda}, \tag{1}$$

where w_0 is the beam radius at the focal plane.

To determine the depth of focus, we translated the imaging system, which is positioned on a translation stage, through the focus with steps of 0.5 μm, while recording the maximum intensity at the focal spot. The results are shown in Fig. 9. A clear peak can be distinguished above the noise floor governed by the surrounding speckle modulation (denoted by the red line). The FWHM of the peak that emerges from this data corresponds with the depth of focus and half of this measure, which is the Rayleigh length, is equal to $z_R = (2.0 \pm 0.5)$ μm and

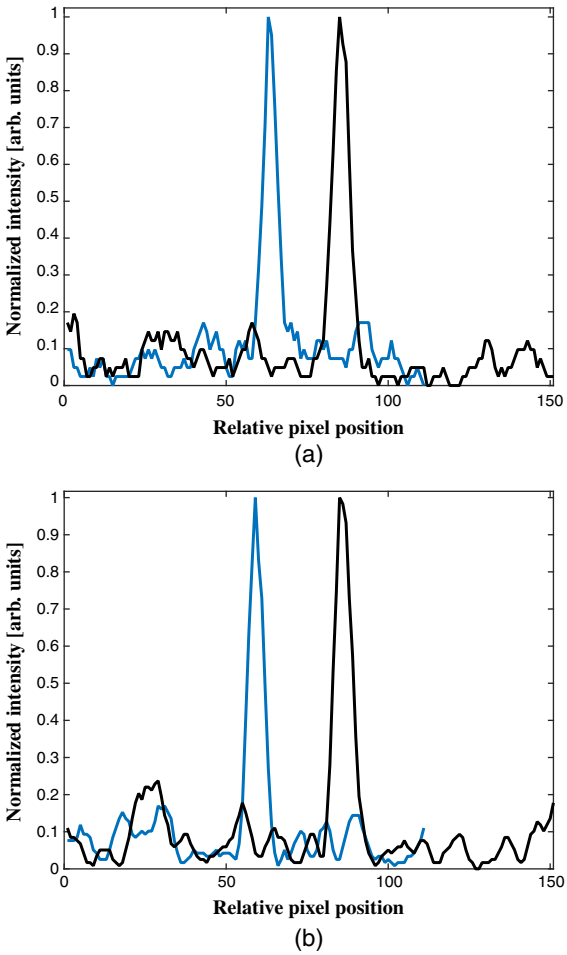

Fig. 8. Normalized line scans through focal spots obtained in (a) lateral and (b) transversal configuration. Line scans taken through x (blue) and y (black) direction.

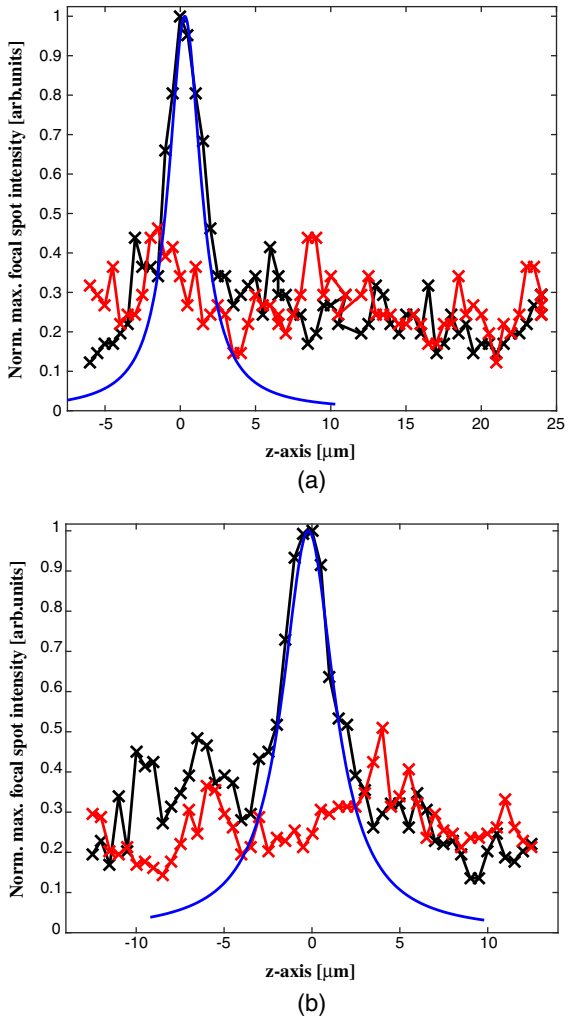

Fig. 9. Normalized maximum intensity of focal spot while scanning through the depth of focus of focal spots obtained in (a) lateral and (b) transversal configuration. Black line is the measured data, red line denotes the background speckle modulation, and the blue line is the theoretical fit.

Table 5. Results for Transversal and Lateral Focusing Configuration

	Configuration	
Parameter	Transversal (μm)	Lateral (μm)
FWHM $w_{0,\text{experimental}}$ (Fig. 8)	0.7 ± 0.1	0.6 ± 0.1
½ of $1/e^2 w_{0,\text{experimental}}$	0.6 ± 0.1	0.5 ± 0.1
$z_{R,\text{experimental}}$ (Fig. 9)	2.0 ± 0.5	1.6 ± 0.5
$z_{R,\text{theoretical}}$ [Eq. (1)]	1.8 ± 0.1	1.3 ± 0.1

$z_R = (1.6 \pm 0.5)$ μm for lateral and transversal configuration, respectively. The error margin is determined by the scanning distance of the translation stage. These results are summarized in Table 5.

5. DISCUSSION

The speckle transverse dimension as a function of distance from the diffuser is governed purely by diffraction (so-called deep Fresnel zone), diffraction and divergence (Fresnel zone), and pure divergence (Fraunhofer zone). The latter two zones can be joined into one zone called the Van–Cittert–Zernicke zone (VCZ). The speckle transverse dimension δx in the VCZ is given by $\delta x = \lambda z/D$, where z is the observation distance and D is the dimension of the illuminated spot [21]. This is strictly valid in the paraxial approximation, which is achieved if $z \gg D$ or, in the case where $z < D$, provided the diffraction angle θ from the diffuser is smaller than ~ 10 deg($\sin(\theta) \sim \theta$). For distances closer to the diffuser, in the deep Fresnel zone, the speckle size is purely determined by diffraction and shows no dependence on the distance z from the diffuser nor on its thickness [22]. The separation between both regions is given by the width of the coherence factor μ_0, which can be approximated by the grain size δx_0 of the diffuser [21,23]:

$$z_{\mathrm{VCD}} = \frac{\mu_0 D}{\lambda} \simeq \frac{\delta x_0 D}{\lambda}. \quad (2)$$

In order to understand the observed speckle size of Table 5, one therefore needs to determine in which region one is operating.

The Teflon sample of 2 mm thickness has a transport mean free path of 600 μm, indicating that diffusion and multiple scattering occurs inside the sample, so that emerging light rays are completely randomized at the exit surface, resulting in a Lambertian emission. The equivalent grain size that generates this emission pattern is, as calculated purely from diffraction, $\delta x_0 = \lambda/2$, approximately 0.3 μm, given the He–Ne wavelength used in our experiment. The obtained limit using equation (2) is $z_{\mathrm{VCZ}} = 3$ mm–4 mm. We therefore find that both measurements, at 0 deg and at 90 deg, are well within the deep Fresnel zone. This explains why both measurements show approximately the same values for z_R and w_0 (within our resolution). If the measurements were done in the VCZ zone, one would expect four times larger speckles for the direct measurement at zero degrees, given the four times longer distance to the focal plane.

As shown by [24], the intensity profile of the focus has the shape of the speckle correlation function, which in the case of a Gaussian radiation source (He–Ne laser) is also Gaussian. The diameter w of the focus speckle also propagates as a function of the distance from its beam waist w_0 at z_0 as a Gaussian beam, and the center intensity drops, therefore, to $1/2$ after a distance equivalent to the Rayleigh length z_R. This again agrees well with the obtained results in Table 5 (line 4).

6. CONCLUSION

In summary, we have proposed and demonstrated an alternative experimental setup to focus light through a multiple scattering sample using wavefront shaping. Within the proposed lateral setup, focusing occurs at a 90 deg angle relative to the sample, which is in contrast to the usual setup for scattering lenses used so far, where focusing is obtained behind the scattering sample (transversal setup). We demonstrate that the depth of focus in transversal and lateral configurations is comparable because both setups are designed to operate in the deep Fresnel zone. This finding suggests that this versatile, lateral setup might be employed in novel applications involving focusing and imaging around the corners of multiple scattering media.

Funding. Conselho Nacional de Desenvolvimento Científico e Tecnológico (CNPq) (2012/402241, 2012/401580, 303286/2013-0); Coordenação de Aperfeiçoamento de Pessoal de Nível Superior (CAPES) (BEX 1497/14-6); Fundação de Amparo à Pesquisa do Estado de São Paulo (FAPESP) (2012/18162-4, 2013/01805-2).

REFERENCES

1. D. S. Wiersma, "Disordered photonics," Nat. Photonics **7**, 188–196 (2013).
2. E. Akkermans and G. Montambaux, *Mesoscopic Physics of Electrons and Photons* (Cambridge University, 2007).
3. D. S. Wiersma, "The physics and applications of random lasers," Nat. Phys. **4**, 359–367 (2008).
4. V. Ntziachristos, "Going deeper than microscopy: the optical imaging frontier in biology," Nat. Methods **7**, 603–614 (2010).
5. P. Sebbah, *Waves and Imaging Through Complex Media* (Springer, 2001).
6. M. Vellekoop and A. P. Mosk, "Focusing coherent light through opaque strongly scattering media," Opt. Lett. **32**, 2309–2311 (2007).
7. I. M. Vellekoop, A. Lagendijk, and A. P. Mosk, "Exploiting disorder for perfect focusing," Nat. Photonics **4**, 320–322 (2010).
8. A. P. Mosk, A. Lagendijk, G. Lerosey, and M. Fink, "Controlling waves in space and time for imaging and focusing in complex media," Nat. Photonics **6**, 283–292 (2012).
9. Y. M. Wang, B. Judkewitz, C. A. DiMarzio, and C. Yang, "Deep tissue focal fluorescence imaging with digitally time-reversed ultrasound-encoded light," Nat. Commun. **3**, 928 (2012).
10. O. Katz, E. Small, Y. Bromberg, and Y. Silberberg, "Focusing and compression of ultrashort pulses through scattering media," Nat. Photonics **5**, 372–377 (2011).
11. F. van Beijnum, E. G. van Putten, A. Lagendijk, and A. P. Mosk, "Frequency bandwidth of light focused through turbid media," Opt. Lett. **36**, 373–375 (2011).
12. Y. Guan, O. Katz, E. Small, J. Zhou, and Y. Silberberg, "Polarization control of multiply-scattered light through random media by wavefront shaping," Opt. Lett. **37**, 4663 (2012).
13. M. Leonetti and C. López, "Active subnanometer spectral control of a random laser," Appl. Phys. Lett. **102**, 071105 (2013).
14. M. Leonetti and C. Conti, "Observation of three dimensional optical rogue waves through obstacles," Appl. Phys. Lett. **106**, 254103 (2015).
15. J. Bertolotti, E. G. van Putten, C. Blum, A. Lagendijk, W. L. Vos, and A. P. Mosk, "Non-invasive imaging through opaque scattering layers," Nature **491**, 232–234 (2012).
16. T. Cizmar, M. Mazilu, and K. Dholakia, "In situ wavefront correction and its application to micromanipulation," Nat. Photonics **4**, 388–394 (2010).
17. A. Velten, T. Willwacher, O. Gupta, A. Veeraraghavan, M. G. Bawendi, and R. Raskar, "Recovering three-dimensional shape around a corner using ultrafast time-of-flight imaging," Nat. Commun. **3**, 745 (2012).
18. O. Katz, E. Small, and Y. Silberberg, "Looking around corners and through thin turbid layers in real time with scattered incoherent light," Nat. Photonics **6**, 549–553 (2012).

19. M. Vellekoop and A. P. Mosk, "Phase control algorithms for focusing light through turbid media," Opt. Commun. **281**, 3071–3080 (2008).
20. H. Yilmaz, W. L. Vos, and A. P. Mosk, "Optimal control of light propagation through multiple-scattering media in the presence of noise," Biomed. Opt. Exp. **4**, 1759–1768 (2013).
21. J. W. Goodman, *Statistical Optics* (Wiley, 2000).
22. M. Giglio, M. Carpineti, and A. Vailati, "Space intensity correlations in the near field of the scattered light: a direct measurement of the density correlation function g(r)," Phys. Rev. Lett. **85**, 1416–1419 (2000).
23. D. Magatti, A. Gatti, and F. Ferri, "Three-dimensional coherence of light speckles: experiment," Phys. Rev. A **79**, 05831 (2009).
24. R. Cerbino, "Correlations of light in the deep Fresnel region: an extended Van Cittert and Zernike theorem," Phys. Rev. A **75**, 053815 (2007).